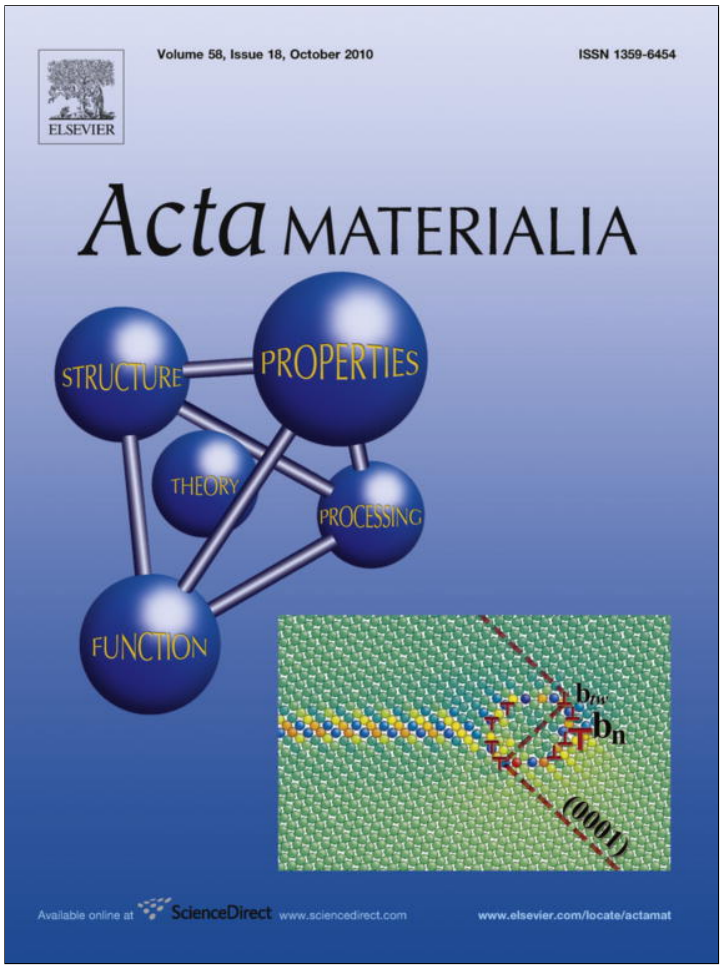

Available online at www.sciencedirect.com
ScienceDirect
Acta Materialia 58 (2010) 6104–6114
Acta MATERIALIA
www.elsevier.com/locate/actamat

Hierarchical magnesium nano-composites for enhanced mechanical response

Meisam K. Habibi, Shailendra P. Joshi, Manoj Gupta *

Department of Mechanical Engineering, National University of Singapore, 9 Engineering Drive 1, Singapore 117576, Singapore

Received 15 June 2010; received in revised form 15 July 2010; accepted 16 July 2010
Available online 10 August 2010

Abstract

In this work we have synthesized and investigated the mechanical performance of a hierarchical magnesium (Mg) nano-composite with a novel micro-architecture including a reinforcing constituent that is a composite in itself. Specifically, we developed a nano-composite (alternatively referred to as a level II composite) with monolithic Mg as the matrix, reinforced by another level I composite comprising a sub-micron pure aluminum (Al) matrix in which are embedded nano-alumina (n-Al_2O_3) particles. The level II composite was obtained by adding a small volume fraction (vf) of the ball-milled level I composite to Mg using the powder metallurgy route followed by microwave-assisted rapid sintering and hot extrusion. Compared with the monolithic pure Mg, the hierarchical composites exhibited significant simultaneous enhancement of strengthening, hardening and failure strain, and also non-monotonic mechanical performance as a function of level I vf. Among the different hierarchical formulations synthesized, the hierarchical level I composition with 0.972% Al and 0.66% Al_2O_3 by volume (Mg/0.972 Al–0.66 Al_2O_3) exhibited the best overall mechanical properties compared with monolithic Mg, with an improvement of 96% in the 0.2% yield strength, 80% in the ultimate tensile strength, 42% in failure strain and 147% in the work of fracture. We identified and quantified some of the strengthening mechanisms that may be responsible for the impressive performance of this hierarchical nano-composite.

Keywords: Magnesium metal matrix composite; Hierarchical nano-composite; Powder metallurgy; Ball milling; Al and Al_2O_3 reinforcements

1. Introduction

Magnesium is an excellent candidate for weight critical structural applications because of its impressively low mass density that renders a high specific stiffness and strength. It also possesses good dimensional stability, a high damping capacity and good high temperature creep properties [1–4]. However, Mg and its alloys are elastically and plastically softer than most Al alloys, which are popular in protean applications ranging from the automotive to defense sectors. One way to enhance the strength of Mg is to reinforce it with stronger inclusions in the form of particles or fibers, essentially forming composite microstructures. However, the end properties of Mg composites are governed by a number of factors, such as the type of processing, matrix constitution, and type, size, volume fraction (vf) and morphology of the reinforcement, secondary processing and heat treatment procedure [5,6]. Among these, selection of a reinforcement compatible with the metallic matrix is an important aspect in realizing useful properties of the resulting composite. For example, it may be possible to achieve higher strengths by increasing the reinforcement vf, but this usually occurs at the cost of reduced ductility. Recent studies have indicated that addition of a dilute vf of nano-sized reinforcements such as alumina (Al_2O_3), silicon carbide (SiC) or carbon nanotubes can lead to a simultaneous increase in strength and ductility of Mg composites compared with monolithic Mg [4–8]. This has been attributed to so-called non-continuum size effects that occur due to enhanced interactions between the inclusions and dislocations [4,5,7,8]. In a novel experiment, Zhong et al. [9]

* Corresponding author. Tel.: +65 6516 6358.
E-mail address: mpegm@nus.edu.sg (M. Gupta).

1359-6454/$36.00 © 2010 Acta Materialia Inc. Published by Elsevier Ltd. All rights reserved.
doi:10.1016/j.actamat.2010.07.028

reported enhanced strength and ductility of pure Mg on incorporating a small vf of ductile nano-aluminum (n-Al) particles as reinforcement using a powder metallurgy approach. They observed that increasing the n-Al vf systematically increased both the strength and ductility, however, beyond a critical vf both these properties may be compromised. This is also true for Mg composites including stiff elastic ceramic reinforcements [7,8].

Motivated by the significant enhancements in the mechanical response of Mg achieved through protean types of nano-scaled reinforcement, we asked what if the stiff elastic inclusions were judiciously integrated into a compatible softer, sub-micron metallic reinforcement and then that was embedded within the Mg matrix? The resulting composite would possess an inherently hierarchical microstructure involving multiple constituents at different length scales, a concept commonly found in natural microstructures (e.g. nacre in abalone shell). The degrees of freedom in such a design may provide an exciting route to engineering the behavior of Mg composites. In this work we demonstrate that such a hierarchical Mg microstructure indeed exhibits excellent mechanical properties derived from superposition of the deformation mechanisms active at small length scales [10]. Schoenung and co-workers [11] developed trimodal micro-architectures of Al alloy metal matrix composites by tuning their grain size distribution and engineering the topological arrangement of the particulate reinforcement. The proposed architecture in this work may also be visualized as a novel trimodal Mg alloy. To the best of our knowledge, such a microstructural design integrating a nano-scaled ductile composite into a Mg matrix has not been previously attempted.

To illustrate the efficacy of the hierarchical Mg microstructure and enable interpretation of the experimental observations, we choose nominally pure forms of Mg, Al and Al_2O_3 as model constituents. This was also motivated keeping in mind the favorable mechanical response of Mg individually with particles of Al and n-Al_2O_3, as previously shown [8,9]. Besides being available at low cost, Al_2O_3 exhibits excellent oxidation resistance, high specific stiffness and superior high temperature mechanical properties, which are even higher in nano-scale structures [12]. Details of the synthesis are discussed in the next section, but Fig. 1 illustrates the underlying concept. The sub-micron Al and n-Al_2O_3 were combined through a ball milling process giving us the level I composite, which was then combined with pure Mg to form a level II nano-composite. In the present work emphasis was placed on investigating the effect of the ball milled Al–Al_2O_3 (i.e. level I composite) on the mechanical response, including the strengthening and ductility, of the level II (i.e. Mg + level I) nano-composite.

In the following sections we describe the synthesis technique to achieve the hierarchical microstructure and discuss the microstructure–properties relationship, including strengthening and failure.

2. Experimental procedures

2.1. Materials

Mg powder (98.5% purity, 60–300 μm particles size range) supplied by Merck (Germany) was used as the matrix material. Alumina powder (50 nm average particles size) supplied by Baikowski (Japan) and aluminum powder (7–15 μm particles size range) supplied by Alfa Aesar (USA) were used as the reinforcements.

2.2. Processing

2.2.1. Preparation of composite reinforcements

In order to prepare different reinforcements for different nano-composite formulations the content of Al_2O_3 particles was kept constant at 0.66% vf [8] while the Al was varied. Stearic acid (0.3 wt.%) was used as the process control agent (PCA). In the first stage, Al and Al_2O_3 particles were blended with stearic acid for 1 h using a Retsch PM-400 mechanical alloying machine. In the second stage, steel balls were added and the blended mixture was ball milled for 2 h. The ball to powder ratio was kept at 20:1 and the speed of the milling machine was set at 200 rpm during the blending and ball milling steps. Blending ensured a uniform distribution of the Al and Al_2O_3 particles. However, it is not possible to embed nano-scaled Al_2O_3 in sub-micron sized Al simply by blending; this requires severe plastic work. To realize this, a ball milling step was introduced. Due to the inherent nature of ball milling, which involves repeated flattening, cold welding, fracture and rewelding of the softer metallic phase, the brittle Al_2O_3 was effectively embedded in Al particles [13]. Based on earlier studies [14,15], it was expected that the level I composite synthesized in the present study would be more reactive compared with the initial constituents, due to the large lattice strains arising from the generation of dislocations and crystal defects during the ball milling step. This could result in the formation of intermetallic phases, which may assist in strengthening.

2.2.2. Primary processing

The hierarchical Mg nano-composites were synthesized using the powder metallurgy technique. The synthesis process involved blending pure Mg powder with the ball-milled level I composite particles in a Retsch PM-400 mechanical alloying machine at 200 rpm for 1 h. The blended powder mixture was compacted at a pressure of 97 bar (load 50 tons) into billets (40 mm height, 35 mm diameter) using a 100 tons press. The compacted billets were sintered using a hybrid microwave assisted two-directional sintering technique. The billets were heated for 13 min to a temperature near the melting point of Mg in a 900 W, 2.45 GHz Sharp microwave oven using colloidal graphite as an oxidation barrier layer. This resulted in a sintered compact of the level II nano-composite, which

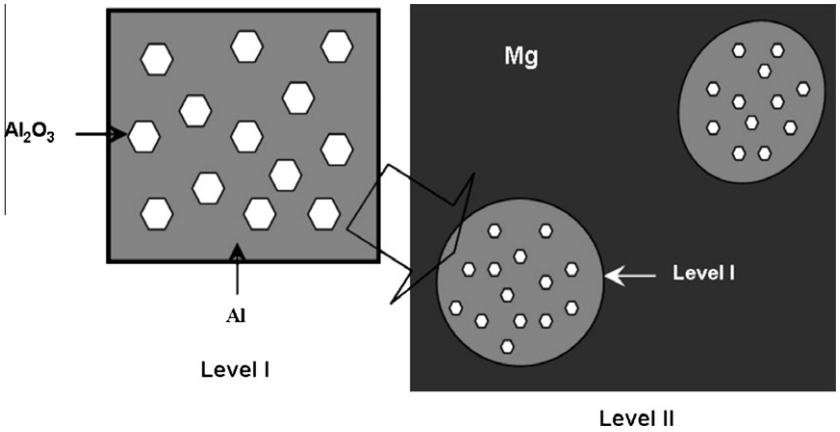

Fig. 1. Schematic of the hierarchical Mg nano-composite synthesized in this work.

was subjected to further processing in order to minimize the porosity.

2.2.3. Secondary processing

The sintered billets of the level II nano-composite were hot extruded at a temperature of 350 °C with an extrusion ratio of 25:1 using a 150 tons hydraulic press. Before extrusion the billets were coated with colloidal graphite and soaked at 400 °C for 1 h. The final diameter of the rods obtained after extrusion was 7 mm.

2.3. Density measurements

The mass densities of the extruded level II nano-composites in the as-polished condition were determined using Archimedes principle [3]. The samples were weighed in air and then immersed in distilled water using an A&D ER-182A electronic balance with an accuracy of ±0.0001 g. The theoretical mass densities of the samples were calculated using the rule of mixtures, assuming that there was no Mg/Al–Al_2O_3 interfacial reaction. The theoretical densities used in calculating the overall nano-composite density were 1.74 g cm^{-3} (Mg), 2.699 g cm^{-3} (Al) and 3.98 g cm^{-3} (Al_2O_3). Table 1 gives the results of density measurements. The measured nano-composite densities were very close to the theoretical values. Thus, near dense nano-composites could be consistently obtained using the fabrication methodology adopted in the present study. However, for Al amounts greater than the ~1.0% considered in this work the porosity fraction is appreciably larger than with Al amounts smaller than ~1.0%, which may adversely affect the mechanical stability of the nano-composites.

2.4. Microstructural characterization

Microstructural characterization studies were conducted on polished samples of monolithic pure Mg and its nano-composite formulations to determine the grain size, grain morphology and the presence and distribution of reinforcements. A Hitachi FE-4300 field emission scanning electron microscope equipped for energy dispersive X-ray spectroscopy (EDS), an Olympus metallographic optical microscope and Scion image analysis software were used for this purpose.

X-ray diffraction (XRD) analysis was carried out on the polished samples and the ball milled composite reinforcement using an automated Shimadzu LAB-X XRD-6000 diffractometer. The samples were exposed to Cu Kα radiation (λ = 1.54056 Å) at a scanning speed of 2 deg min^{-1}.

2.5. Hardness measurement

Micro-hardness measurements were made on the polished samples of extruded monolithic and hierarchical Mg rods using a Matsuzawa MXT 50 automatic digital micro-hardness tester. The micro-hardness tests were performed using a Vickers indenter under a test load of 25 gf and a dwell time of 15 s in accordance with the ASTM standard E3 84-99. Table 2 compares the micro-hardness of the pure Mg and hierarchical Mg samples with varying amounts of Al. The latter exhibited significantly greater hardnesses compared with the former. However, the difference in hardness between various level II formulations was not significant considering their standard deviations. This enhanced micro-hardness may be attributed primarily to:

Table 1
Results of the density and porosity measurements.

Material	Reinforcement (vol.%) (Al, Al_2O_3)	Theoretical density (g cm^{-3})	Experimental density (g cm^{-3})	Porosity (%)
Mg		1.7400	1.7379 ± 0.005	0.12
Mg/0.647 Al–0.66 Al_2O_3	0.647, 0.660	1.7611	1.7599 ± 0.003	0.06
Mg/0.972 Al–0.66 Al_2O_3	0.972, 0.660	1.7642	1.7633 ± 0.020	0.05
Mg/1.298 Al–0.66 Al_2O_3	1.298, 0.660	1.7673	1.7638 ± 0.012	0.20
Mg/1.950 Al–0.66 Al_2O_3	1.950, 0.660	1.7736	1.7648 ± 0.015	0.34

Table 2
Results of grain morphology and hardness.

Material	Grain size (μm)	Aspect ratio	Micro-hardness (HV)
Mg	19 ± 4	1.5 ± 0.3	40 ± 2
Mg/0.647 Al–0.66 Al_2O_3	8 ± 4	1.7 ± 0.5	59 ± 4
Mg/0.972 Al–0.66 Al_2O_3	8 ± 4	1.7 ± 0.4	60 ± 3
Mg/1.298 Al–0.66 Al_2O_3	7 ± 4	1.8 ± 0.6	62 ± 4
Mg/1.950 Al–0.66 Al_2O_3	7 ± 3	1.7 ± 0.5	62 ± 3

(a) the presence of relatively harder nano-particles in the matrix [3,4]; (b) a higher constraint to localized matrix deformation during indentation due to the presence of the level I composite [3,4]; (c) a reduced Mg grain size (Table 2) [3,4,16]. The results further reveal that in this case the level I vf did not significantly affect the hardness of the bulk samples (Table 2).

2.6. Tensile tests

The smooth bar tensile properties of the monolithic and hierarchical Mg extruded rods were determined based on ASTM E8M-05. Round tension test samples of 5 mm in diameter and 25 mm gauge length were subjected to tensile loading using an automated servo-hydraulic testing machine (MTS 810) with a cross-head speed set at 0.254 mm min^{-1}, giving a nominal strain rate of about 1.67×10^{-4} s^{-1}. A clip-on extensometer was used to measure the nominal strain.

3. Results

3.1. Macrostructural characteristics

Macrostructural characterization conducted on the as-sintered billets revealed an absence of macrostructural defects such as circumferential or radial cracks. Following extrusion no observable macroscopic defects were observed on the surfaces of the monolithic Mg and hierarchical composite rods. The outer surfaces were smooth and free of any circumferential cracks.

3.2. Microstructural characteristics

Microstructural characterization studies conducted on nano-composite samples indicated a reasonably uniform distribution of the level I composite ($Al + Al_2O_3$) in the Mg matrix up to 0.972 vol.% Al (Fig. 2a and b). Increasing the reinforcement content caused an increase in both porosity and reinforcement clustering (Fig. 2c and d). Fig. 3 shows that the ball milled reinforcement comprised Al (gray scale) speckled with Al_2O_3 (white) particles (i.e. the alumina particles resided entirely in the Al and were not transferred to the Mg matrix during processing). The average Mg grain size in the level II nano-composite was significantly smaller than in the pure Mg (Table 2), suggesting an ability of the level I composite to serve either as nucleation sites or obstacles to grain growth during processing. A near equiaxed grain morphology was observed for both the monolithic and nano-composite samples, indicating that the aspect ratio of the Mg grains was not influenced by addition of the level I composite.

Fig. 4a and b shows the results of the XRD studies conducted on the level I and level II composite, respectively. The XRD results for the ball milled reinforcement revealed the presence of both the Al and Al_2O_3 phases (Fig. 4a), however, the XRD results of the extruded level II nano-composite samples (Fig. 4b) do not explicitly show the presence of Al, Al_2O_3 or any related phases. This may be attributed to the low level I composite vf ($\leqslant$2.5%) within the level II nano-composite. Thermodynamically, it is possible that some Al could form a solid solution with the Mg. However, the absence of any discernable shifts in the XRD peaks in all the hierarchical configurations with respect to those of the pure Mg indicates that Al did not form a solid solution (Fig. 4b). Further, the field emission scanning electron microscopy (FESEM) investigations (Fig. 3) clearly indicated the presence of level I composite giving the expected hierarchical microstructure. In a nutshell, while it is thermodynamically possible for the Al to form a solid solution, the microwave sintering may not provide the necessary kinetics for such a process, as the sintering was very rapid [9].

The uniform distribution of the ball-milled level I composite particles in the level II nano-composite, at least for Al amounts up to 0.972%, may be attributed to: (a) adequate blending parameters and (b) the high extrusion ratio used in the secondary processing. In theory, a homogeneous distribution of the reinforcement should be achievable irrespective of the size difference between the matrix powder and the reinforcement, provided a large deformation load is applied during secondary processing [9]. However, at higher level I vf the observed clustering may be due to the high surface energy of the ball-milled level I composite particles, associated with their large surface area, which warrants further investigation.

3.3. Tensile behavior

Fig. 5a shows the uniaxial, tensile true stress–true strain curves of the hierarchical nano-composite samples for different Al vf along with the response of monolithic Mg. At least six specimens for each composition were tested at a nominal quasi-static strain rate of 1.674×10^{-4} s^{-1}. Fig. 5b (see also Table 3) clearly shows significant improvements in the specific strengths (strength/measured density) and failure strains of the hierarchical nano-composites compared with the monolithic Mg with increasing vf of Al in the level I composite. It is interesting to note, however, that this improvement was not monotonic. For a fixed Al_2O_3 vf within the level I composite the 0.2% yield strength (YS), ultimate tensile strength (UTS) and failure strain (FS) of the hierarchical nano-composites increased monotonically up to an Al fraction of 0.972%. Further increasing the Al

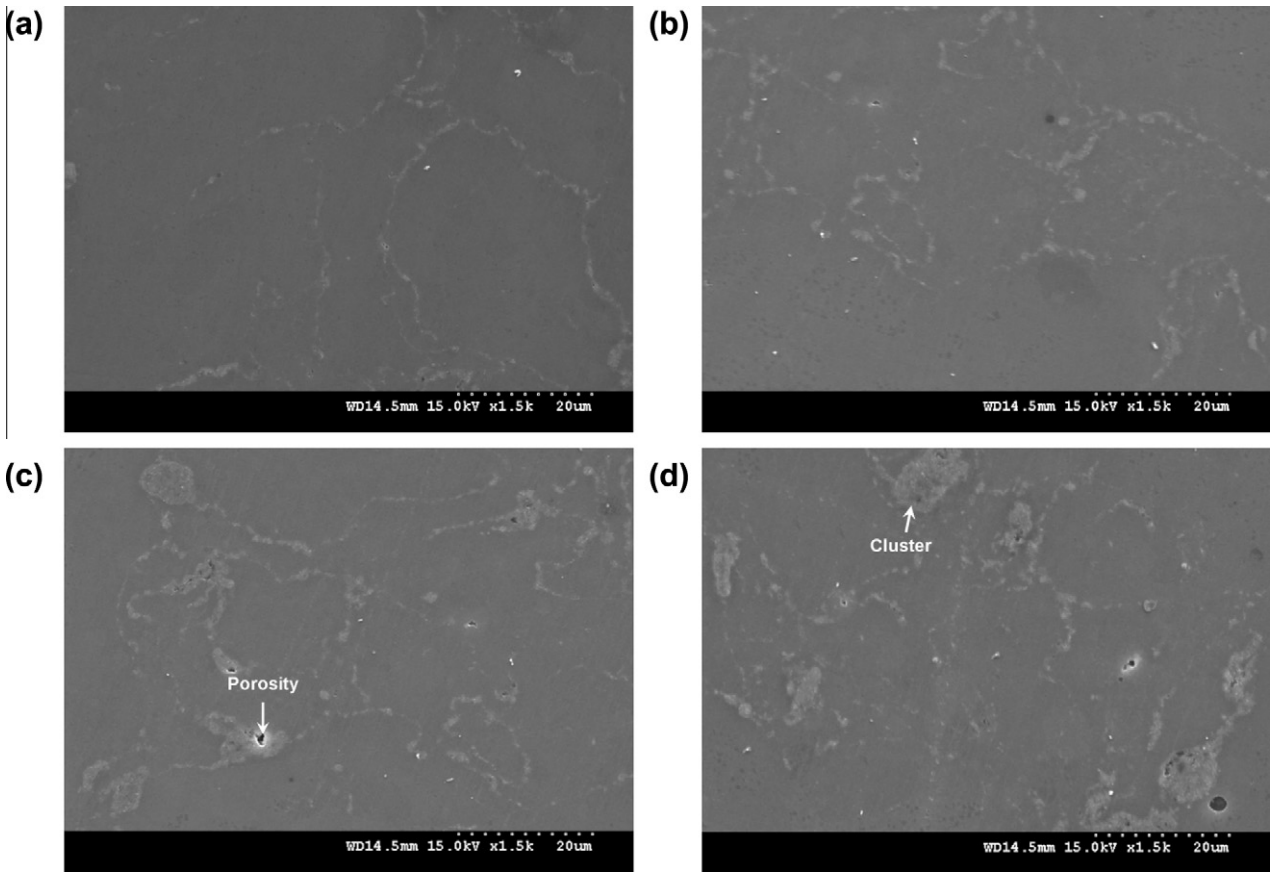

Fig. 2. Representative micrographs showing the distribution of ball-milled level I particles through the matrix in (a) Mg/0.647 Al–0.66 Al_2O_3, (b) Mg/0.97 Al–0.66 Al_2O_3, (c) Mg/1.298 Al–0.66 Al_2O_3 and (d) Mg/1.95 Al–0.66 Al_2O_3 nano-composites.

vf led to a drop in the failure strain, when compared with monolithic Mg. As is evident from Table 3, the hierarchical nano-composites exhibited an overall superior response from the viewpoint of work of fracture (WOF) compared with pure Mg. Among the different hierarchical Mg nano-composites synthesized in this work the Mg/0.972 Al–0.66 Al_2O_3 combination showed the best overall improvement over monolithic Mg, with an impressive increase of 96% in YS, 80% in UTS, 42% in FS and 147% in WOF. We believe that the decrease in strength and ductility with a further increase in the Al vf is largely due to the higher porosity and reinforcement clustering compared with its lower vf counterparts (Table 1 and Fig. 2).

Fig. 6 shows the tensile fracture surfaces of the monolithic and hierarchical nano-composite Mg samples, respectively, performed using a Hitachi FE-4300 field emission scanning electron microscope. The fracture surfaces of the monolithic Mg specimens indicated the presence of cleavage steps (Fig. 6a). However, fracture studies conducted on the hierarchical nano-composite specimens (Fig 6b–e) revealed a mixed failure mode, suggesting plastic deformation modes of the Mg matrix different from that of monolithic Mg. We shed some light on this aspect in Section 4.2.

4. Discussion

4.1. Strengthening mechanisms

The enhanced strength and hardness observed in the hierarchical nano-composites compared with monolithic Mg is attributed to the presence of the level I composite, which activated multiple strengthening mechanisms acting in tandem [10,11]. These include, but may not be limited to: (a) Orowan strengthening [17,18]; (b) grain size strengthening [18,19]; (c) effective load transfer from the matrix to the reinforcement [7,20]; (d) generation of geometrically necessary dislocations (GNDs) to accommodate the coefficient of thermal expansion (CTE) and elastic modulus mismatch between the Mg matrix and the level I composite [21,22]; (e) activation of non-basal slip modes [23].

The yield strength of a material is determined by the stress required to move existing dislocations in the presence of different types of obstacles. In general, the possible mechanisms listed above may interact with each other. Phenomenological and statistical approaches have been discussed in the literature to account for such synergistic effects [5,24]. Although one may resort to the simplest case

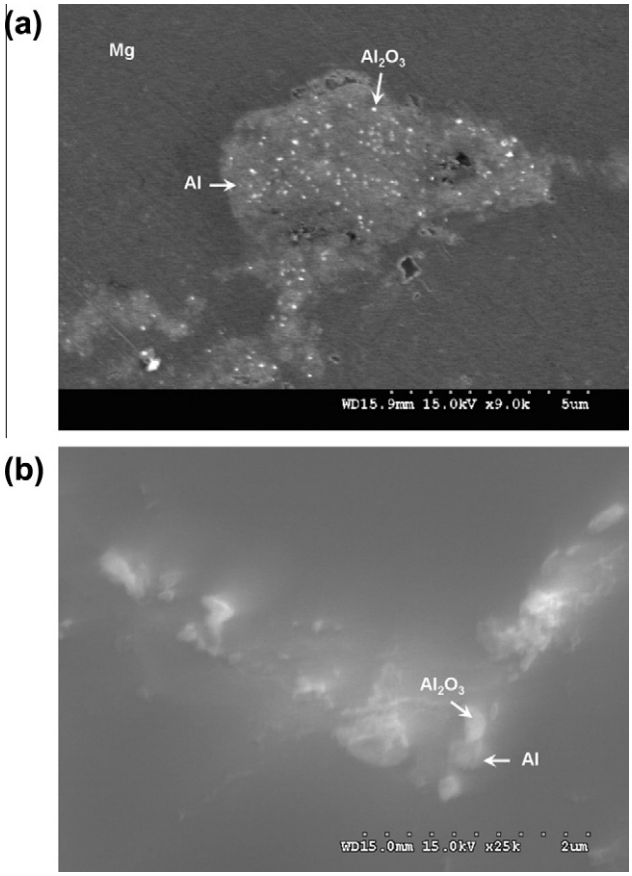

Fig. 3. Level I composite high resolution micrographs showing the coexistence of Al–Al_2O_3 in Mg.

of linear superimposition, the square root sum of squares approach is considered more appropriate when superimposing individual strengthening mechanisms of similar strength [5]. Then the predicted overall yield strength, σ_T, for the level II nano-composite can be expressed as [25]:

$$\sigma_T = \sigma_0 + \sqrt{(\Delta\sigma_{CTE})^2 + (\Delta\sigma_{EM})^2 + (\Delta\sigma_{OR})^2 + (\Delta\sigma_{HP})^2} \quad (1)$$

where σ_0 is the size-independent yield strength of the Mg matrix, $\Delta\sigma_{CTE}$ and $\Delta\sigma_{EM}$ are the GND strengthening contributions, respectively due to a mismatch in the CTE and elastic properties between Mg and the level I composite, $\Delta\sigma_{OR}$ is the Orowan strengthening and $\Delta\sigma_{HP}$ is the grain size strengthening through the Hall–Petch mechanism. Next, we briefly discuss these contributions and provide estimates based on the microstructural characteristics.

4.1.1. GND strengthening

Incompatibilities in plastic deformation may arise within the level II nano-composite due to the CTE mismatch between Mg and the level I composite. This may give rise to GNDs from the thermal residual stresses in the level II nano-composite. The generation of these dislocations leads to an increase in the strength of the material. The strengthening from the CTE mismatch is [25]:

$$\Delta\sigma_{CTE} = A \cdot M \cdot G \cdot b_{Mg} \cdot \rho_{th}^{0.5} \quad (2)$$

where

$$\rho_{th} = \frac{12\sqrt{2} \cdot \Delta\alpha_{II} \cdot \Delta T \cdot f_I}{b_{Mg} \cdot d_I \cdot (1 - f_I)} \quad (3)$$

where ρ_{th} is the GND density for a temperature excursion ΔT (the difference between extrusion temperature and test temperature) due to the CTE mismatch $\Delta\alpha_{II}$ between the Mg matrix and level I inclusions of effective diameter d_I (~300–500 nm as seen in the micrographs). In Eq. (2) A is a constant characterizing the transparency of the dislocation forest for basal–basal dislocation interactions in Mg (~0.2 for Mg) [25], M (=6.5) [26] is the mean orientation (Taylor) factor for Mg and G is the shear modulus (=17.3 GPa), b_{Mg} is the magnitude of the burgers vector for Mg (=0.321 nm) [25] and f_I is the vf of level I inclusions in the level II composite. To calculate $\Delta\alpha_{II}$ ($=\alpha_{Mg} - \alpha_I$) we first need to calculate the CTE of the level I composite α_I; for this we assume the rule of mixtures:

$$\alpha_I = \alpha_{Al_2O_3} f_{Al_2O_3} + \alpha_{Al}(1 - f_{Al_2O_3}) \quad (4)$$

where $f_{Al_2O_3}$ (=0.36) is the vf of Al_2O_3 in Al, $\alpha_{Al} = 26.49 \times 10^{-6}\,K^{-1}$ and $\alpha_{Al_2O_3} = 7.4 \times 10^{-6}\,K^{-1}$.

Similarly, the GND density due to mismatch in the elastic modulus between the Mg matrix and level I inclusions is [10]:

$$\rho_{EM} = \frac{6 f_I \varepsilon}{b d_I} \quad (5)$$

where ε is assumed to be the elastic strain at yield (=0.002). The value of $\Delta\sigma_{EM}$ was obtained using an equation similar to Eq. (2) but with ρ_{EM}.

4.1.2. Orowan strengthening

The Orowan mechanism that accounts for dislocations bowing between obstacles can be an effective strengthening mechanism for inclusions on the sub-micron to nanometer scales. In addition to particle size, a uniform dispersion of particles is preferable in order to have as many particles as possible take part in this strengthening mechanism [27]. Due to the presence of the level I inclusions of sub-micron and nanometer size, residual dislocation loops may be formed around each particle after a dislocation bows out and bypasses it by means of the Orowan mechanism. These loops may lead to high work hardening rates and assist the stability of deformation up to larger strains. The contribution to yield strength from Orowan strengthening can be expressed as [25]:

$$\Delta\sigma_{OR} = \frac{\frac{0.4MGb}{\pi\bar{\lambda}} \ln\left(\frac{d_I}{b}\right)}{\sqrt{1 - \nu_{Mg}}} \quad (6)$$

where ν_{Mg} is the Poisson's ratio for Mg and $\bar{\lambda}$ is the mean inter-particle distance given by $\bar{\lambda} = d_I\left(\sqrt{\frac{4}{\pi f_I}} - 1\right)$ [28].

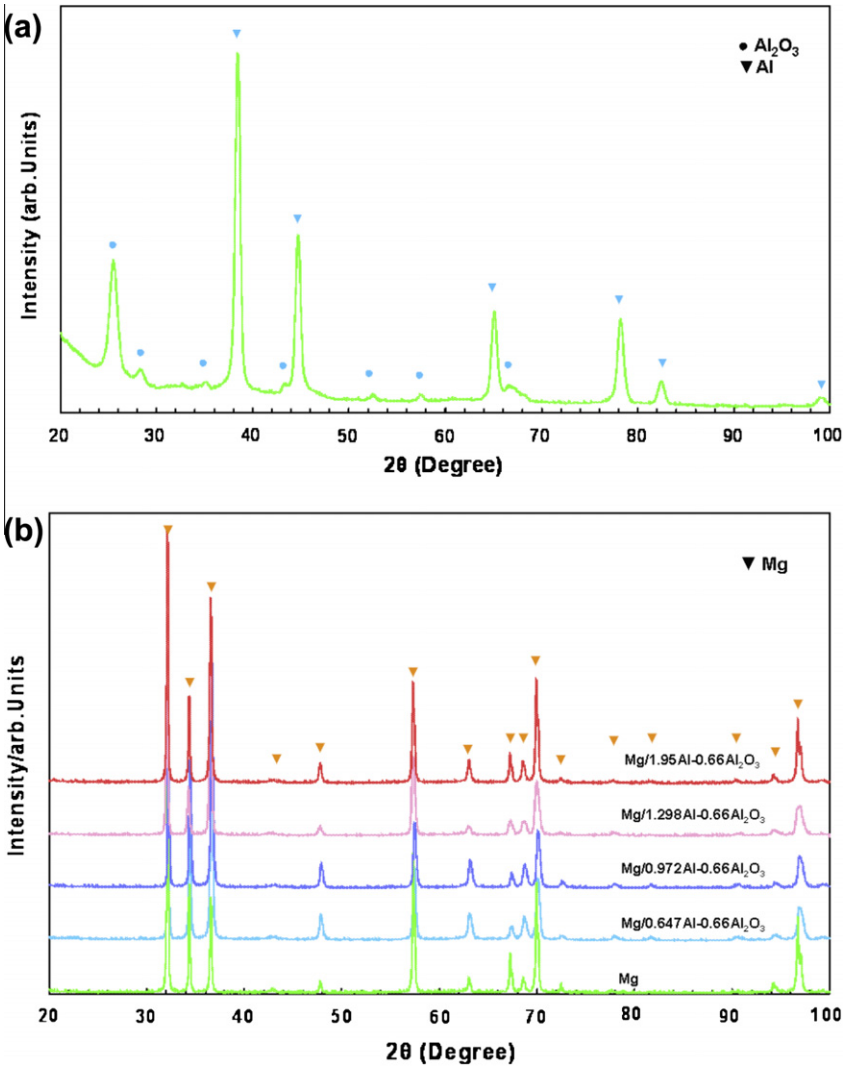

Fig. 4. Representative XRD spectra of (a) level I composite and (b) sintered and extruded level II nano-composites with different level I vf.

4.1.3. Grain size strengthening

Hall–Petch strengthening due to grain size is given by [25]:

$$\Delta\sigma_{HP} = k_y d_{Mg}^{-0.5} \quad (7)$$

where k_y is the Hall–Petch coefficient (280 MPa $\mu m^{1/2}$) [26] and d_{Mg} is the average Mg grain size (Table 2).

4.1.4. Volume fraction effect

In the level II composite load sharing occurring between the softer Mg matrix and the comparatively harder level I inclusions provides strengthening. This depends on two important parameters, namely the interfacial bonding between the inclusion and matrix, and the vf of the inclusion phase. The results suggest that good interfacial bonding exists between Mg and the composite Al–Al_2O_3 particles (Fig. 1). Moreover, it has been established that a low melting point metal is capable of wetting a high melting point metal [29]. This should assist load sharing. However, the second aspect, which is crucial, is the vf of the level I inclusions. Given its dilute fraction in all the hierarchical configurations, the vf effect may play only a minor, if any, role in contributing to the overall strength of the level II composite and is neglected in our calculations.

4.1.5. Activation of non-basal slip

Activation of non-basal slip systems may also be a factor that enhances the strength and hardening of hierarchical Mg nano-composites. As observed from the FESEM micrograph (Fig. 7a) a typical fracture surface of the Mg/0.972 Al–0.66 Al_2O_3 nano-composite shows large serrations compared with monolithic Mg (Fig. 7b) indicating non-basal activity [30]. Non-basal slip modes require much larger resolved shear stresses compared with basal slip [23,30]. The refined grain size in our hierarchical composites may provide sites for local high stresses through heterogeneities in the form of grain boundaries. Further, level I inclusions may also trigger non-basal modes. Our crystal plasticity simulations [31] indicate that, depending on the grain orientation, the presence of an inclusion generates

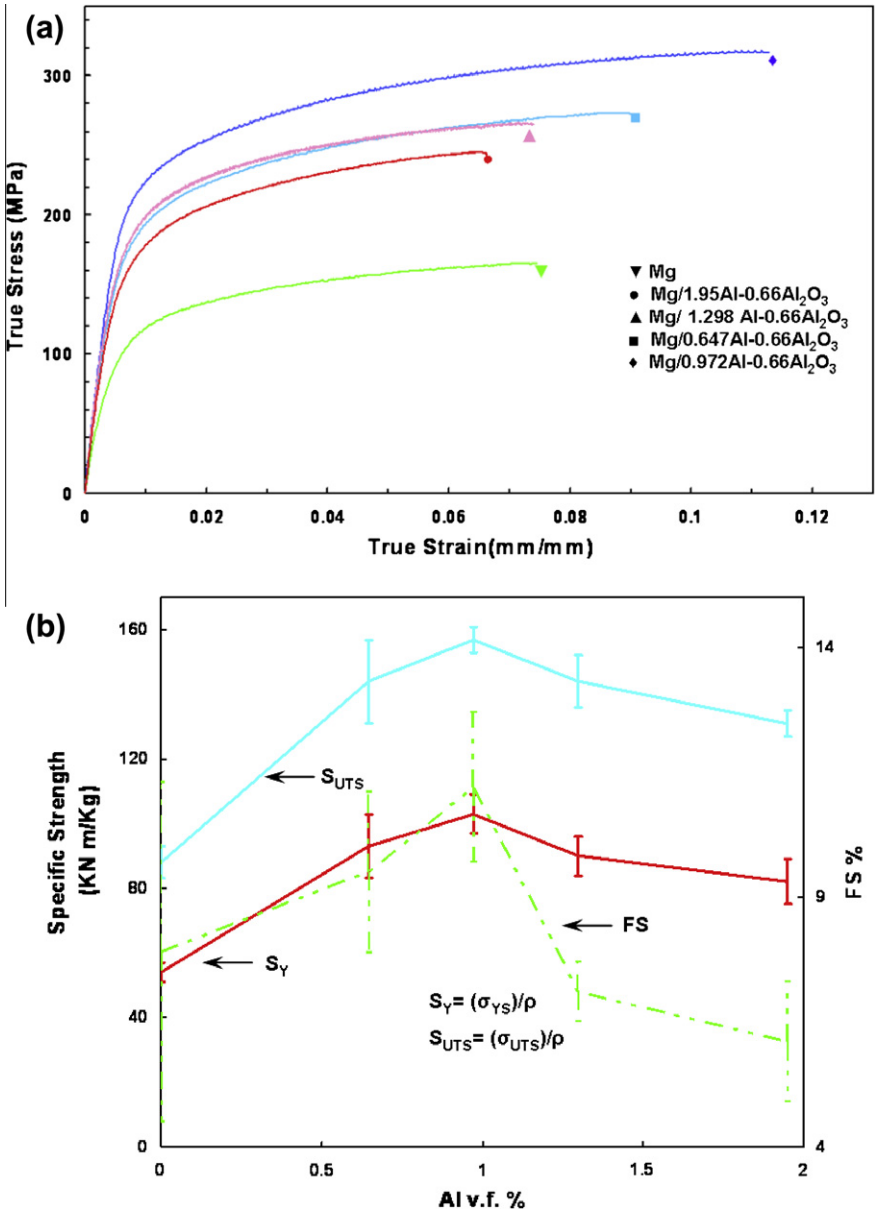

Fig. 5. (a) True stress–true strain curves for monolithic Mg and hierarchical nano-composite specimens. (b) Variation of specific strength and FS with Al vf within the level I composite.

Table 3
Room temperature tensile properties.

Material	0.2% YS (MPa)	UTS (MPa)	Failure strain (%)	WOF (J m^{-3})[a]
Mg	93 ± 01	153 ± 07	7.9 ± 3.4	12 ± 5
Mg/0.647 Al–0.66 Al_2O_3	164 ± 18	254 ± 23	9.5 ± 1.6	24 ± 6
Mg/0.972 Al–0.66 Al_2O_3	182 ± 10	276 ± 08	11.2 ± 1.5	30 ± 3
Mg/1.298 Al–0.66 Al_2O_3	159 ± 11	255 ± 15	7.1 ± 0.6	19 ± 1
Mg/1.950 Al–0.66 Al_2O_3	148 ± 10	233 ± 07	6.1 ± 1.2	14 ± 2

[a] Determined from the stress–strain curves.

high local stresses that are heterogeneous compared with a pure Mg crystal. This in turn triggers a significant amount of pyramidal or prismatic slip activity in a grain. Pyramidal or prismatic slip may also be activated by lattice reorientation if a grain undergoes profuse twinning, initially due to high local stresses. Such non-basal activity may result in strengthening and hardening, even of grains that may otherwise be preferentially oriented for basal slip. The refined grain size was primarily due to the initial plastic work during processing, along with the presence of the nano-scaled level I composite, which effectively stabilizes the microstructure. The level I phase may itself be responsible for activation of non-basal slip modes in its vicinity [23]. As loading continues, the activation of multiple non-basal slip modes likely causes enhanced interaction between these slip systems, leading to overall hardening.

The contributions of the various above mentioned strengthening mechanisms and the synergistic combination of both the level I composite particles and pure Mg account

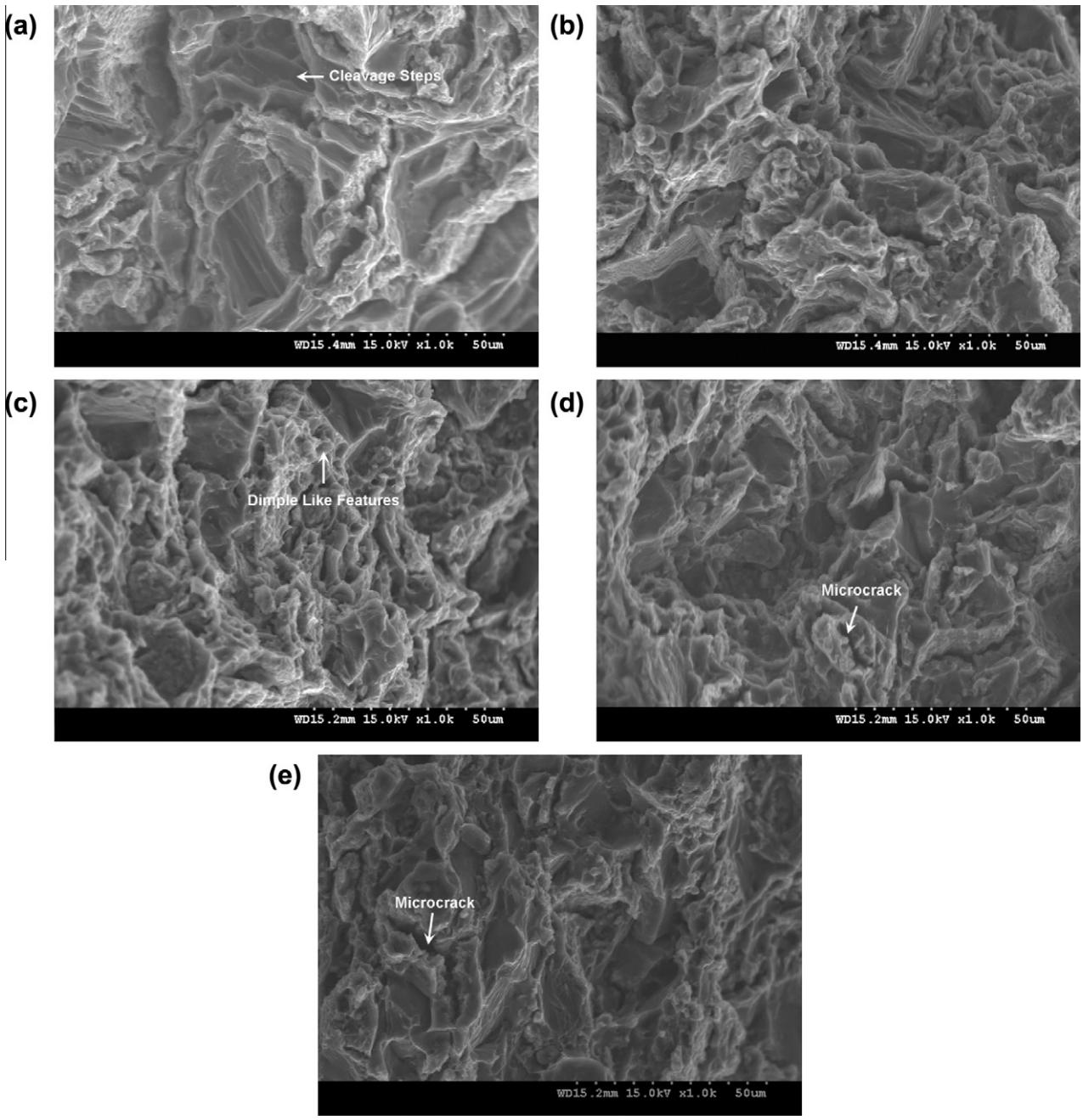

Fig. 6. Representative FESEM micrographs taken from the tensile fracture surfaces showing (a) cleavage steps in pure Mg, mixed fracture mode in (b) Mg/0.647 Al–0.66 Al_2O_3 and (c) Mg/0.972 Al–0.66 Al_2O_3 and formation of a microcrack in (d) Mg/1.298 Al–0.66 Al_2O_3 and (e) Mg/1.95 Al–0.66 Al_2O_3.

for the significant improvement in strength of the hierarchical Mg nano-composites. Using Eqs. (1)–(7) we provide an estimate of the overall strength of Mg/0.972 Al–0.66 Al_2O_3, which showed the best performance among the configurations considered in this work. Table 4 summarizes the individual contributions and the range of the estimated overall strength. We note that the predicted range of strength provides only a rough estimate based on the approximations of microstructural mechanisms mediated by parameters such as d_I, d_{Mg}, $\Delta\alpha_I$ and $\bar{\lambda}$. However, quantification of some of the individual contributions provides a useful sketch of the strengthening mechanisms. These estimates may serve to illustrate the theoretically achievable strengthening, provided precise control of the microstructure is exercised. This will be the focus of future work.

4.2. Failure strain

The increase in failure strain of nano-composites containing composite particles with an Al content of up to 0.972, compared with monolithic Mg, may be attributed to: (a) grain refinement [32], (b) a uniform distribution of level I composite particles [30] and (c) slip of non-basal slip systems (Fig. 7a) [23]. The precipitous reduction in failure strain of

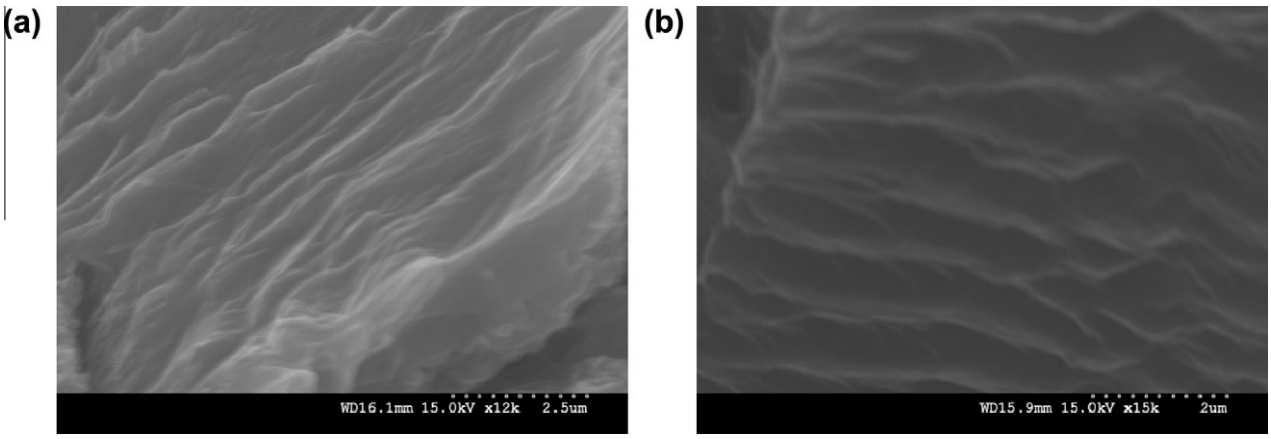

Fig. 7. Representative FESEM fractographs showing (a) uneven lines due to the combined effect of basal and non-basal slip in the case of Mg/0.972 Al–0.66 Al_2O_3 and (b) straight lines due to slip in the basal plane in the case of pure Mg.

Table 4
Contributions of the strengthening mechanisms to the overall composite strength for the Mg/0.972 Al–0.66 Al_2O_3 hierarchical nano-composite.

Component	σ_0	$\Delta\sigma_{CTE}$	$\Delta\sigma_{HP}$	$\Delta\sigma_{OR}$	$\Delta\sigma_{EM}$	Predicted	Actual
Stress (MPa)	93	17.2–37	81–140	11–20	7.9–10	177–239	182 ± 10

the combinations with Al contents greater than 0.972% could result from (i) an increase in the overall porosity (Table 1), (ii) reinforcement clustering (Fig. 1) or (iii) formation of microcracks under tensile loading (Fig. 6d–e).

The fracture surfaces observed in the monolithic Mg sample predominantly reveal the presence of cleavage steps. The presence of cleavage steps indicates an inability of Mg to significantly deform under uniaxial tensile loading, characteristic of the low symmetry hcp structure of Mg (Fig. 6a). However, the fracture surface in the case of the hierarchical nano-composite samples revealed a mixed mode of failure, with evidence of ductile plastic deformation, such as dimples (Fig. 6b–e). As in the case of strengthening, the transition from a brittle to a mixed mode type of fracture may be attributed to the activation of non-basal slip systems [32,33].

5. Conclusions

The conclusions from the current experimental findings are as follows

1. The conventional solid-state powder metallurgy technique with rapid microwave sintering and hot extrusion can be successfully used to synthesize novel hierarchical Mg nano-composites with dilute reinforcement fractions.
2. The hierarchical Mg microstructures synthesized in the present study exhibited a reasonably uniform distribution of level I composite for Al vf up to ~1.0% and low porosity, suggesting adequacy of the processing methodology.
3. The presence of a sub-scale composite (i.e. level I) significantly refined the Mg grain structure and stabilized it by providing pinning sites against grain growth.
4. The specific strengths of all the hierarchical Mg composite compositions synthesized in this work were significantly higher than that of monolithic Mg. Of the combinations synthesized, Mg/0.972 Al–0.66 Al_2O_3 showed the most impressive strengthening, of 96% and 80% for YS and UTS, respectively.
5. The enhancement in strength may be primarily attributed to grain size refinement and Orowan strengthening mechanisms, although synergistic coupling may also occur between different strengthening mechanisms.
6. The hierarchical composite Mg/0.972 Al–0.66 Al_2O_3 was significantly more ductile than monolithic Mg. This can be attributed to the presence and uniform distribution of the level I composite, matrix grain refinement and the activation of non-basal slip modes due to local heterogeneities, as indicated by post-mortem characterization.

Our future work will focus on achieving better control over the processing to minimize the deleterious effects arising from increased porosity and reinforcement clustering. We will simultaneously explore its extension to commercial Mg alloys to assess the efficacy of the hierarchical design concept in improving their overall behavior.

Acknowledgements

S.P.J. and M.G. gratefully acknowledge financial support from the US Army International Technology Center, Pacific through research Contract No. FA5209-10-P-0047

(R-265-000-338-597). S.P.J. also acknowledges partial support through NUS Start-up Grant No. R-265-000-294-133. M.K.H. acknowledges support through a NUS research scholarship.

References

[1] Lloyd DJ. Int Mater Rev 1994;39:1.
[2] Lee DM, Suh BK, Kim BG, Lee JS, Lee CH. Mater Sci Technol 1997;13:590.
[3] Gupta M, Lai MO, Saravanaranganathan D. J Mater Sci 2000;35:2155.
[4] Hassan SF, Gupta M. Mater Sci Technol 2003;19:253.
[5] Clyne TW, Withers PJ. An introduction to metal matrix composites. Cambridge (UK): Cambridge University Press; 1993.
[6] Tham LM, Gupta M, Cheng L. Mater Sci Technol 1999;15:1139.
[7] Hassan SF, Gupta M. Mater Sci Eng A 2006;425:22.
[8] Hassan SF, Gupta M. Mater Sci Eng A 2005;392:163.
[9] Zhong XL, Wong WLE, Gupta M. Acta Mater 2007;55:6338.
[10] Joshi SP, Ramesh KT. Scripta Mater 2007;57:877.
[11] Ye J, Han BQ, Lee Z, Ahn B, Nutt SR, Schoenung JM. Scripta Mater. 2005;53:481.
[12] Ashby MF, Jones DRH. Engineering materials, vol. I. Oxford (UK): Butterworth-Heinemann; 1996.
[13] Suryanarayana C. Mechanical alloying and milling. New York: Marcel Dekker; 2004.
[14] Ernst D, Weiss H, Reichardt R, Zoz H. Mechanical alloying of Fe-based solid lubricant composite powders. The Minerals, Metals and Materials Society; 1998. p. 225.
[15] Lucks I, Lamparter P, Mittemeijer EJ. Acta Mater 2001;49:2419.
[16] Ferkel H, Mordike BL. Mater Sci Eng A 2001;298:193.
[17] Dai LH, Ling Z, Bai YL. Compos Sci Technol 2001;61:1057.
[18] Murr LE. Interfacial phenomena in metals and alloys. Reading (MA): Addison-Wesley; 1975.
[19] Reed-Hill RE. Physical metallurgy principles. New York: D. Van Nostrand Co.; 1964.
[20] Hull D, Bacon DJ. Introduction to dislocations. Oxford (UK): Butterworth-Heinemann; 2002.
[21] Gale W, Totemeier T. Smithells metal reference book. Oxford (UK): Butterworth-Heinemann; 2004.
[22] ASM International. ASM metal reference book. Materials Park (OH): ASM International; 1993.
[23] Pérez P, Garcés G, Adeva P. Compos Sci Technol 2004;64:145.
[24] Nembach E. Acta Metall Mater 1992;40:3325.
[25] Han BQ, Dunand DC. Mater Sci Eng A 2000;277:297.
[26] Wong WLE, Gupta M. Compos Sci Technol 2007;67:1541.
[27] German RM. Powder metallurgy science. Princeton (NJ): Metal Powder Industries Federation; 1994.
[28] Kang YC, Chan SLI. Mater Chem Phys 2004;85:438.
[29] Eustathopoulas N, Nicholas M, Drevet B. Wettability at high temperatures. Amsterdam: Elsevier; 1999.
[30] Ansell GS, Cahn RW. Physical metallurgy. Amsterdam: North-Holland; 1970.
[31] Zhang J, Joshi SP. Crystal plasticity of Mg composites, in preparation.
[32] Koike J, Kobayashi T, Mukai T, Watanabe H, Suzuki M, Maruyama K, et al. Acta Mater 2003;51:2055.
[33] Neite G, Kubota K, Higashi K, Hehmann F. Magnesium based alloys. Weinheim (Germany): Materials Science and Technology; 1996.